CHAPTER 2: OPTICAL PULSE GENERATION

2.1 A Brief History of Laser

The term *laser* is an acronym formed from *l*ight *a*mplification by *s*timulated *e*mission of *r*adiation. Laser emits light coherently. The spatial coherence of a laser allows it to be focused to a tight spot. Its spatial coherence also keeps a laser beam collimated over long distances. Laser also has high temporal coherence that brings about a very narrow spectrum. The temporal coherence also allows laser to emit pulses of light that only last a femtosecond. There are many different kinds of lasers; they all share a crucial element: each contains material capable of amplifying radiation. This material is called the gain medium, simply because radiation gains energy passing through it. Other elements include energy pump and cavity or resonator. In laser physics, the terms cavity and resonator are used interchangeably.

The physical principle responsible for laser is stimulated emission, and was proposed by Einstein in 1916 [1]. In fact, most theoretical foundations of the laser were presented by Einstein. The coefficients for absorption, spontaneous emission and stimulated emission of electromagnetic radiation, which tells the probability of each process, were derived as well. The first laser was constructed by T.H. Maiman in 1960 [2], with the gain medium being a 2 cm long ruby cylinder with 1 cm diameter. The ruby laser was pumped by a xenon flashlight that surrounded the ruby cylinder, having an output at a wavelength of 694.3 nm. Townes, Basov and Prokhorov received the Noble prize in physics for their fundamental work in the field of quantum electronics, which has led to the construction of oscillators and amplifiers based on the maser-laser principle.

Lasers are commonly divided into different categories according to their gain media: solid, liquid or gas. In solid state lasers, the gain medium consists of the host and dopant. The host media can be glass or crystal, which are doped with rare-earth or transitional

metal ion. Fibre lasers are considered as one branch of solid state lasers. The host medium is optical fibre, which is doped with rare-earth ions. Common dopants are ytterbium, erbium and neodymium. Bismuth, praseodymium, dysprosium, thulium and holmium have been used widely as well as gain fibre dopants to explore new wavelength regions. Fibre lasers have several appealing advantages: it is flexible and can be coiled into small spaces. The light is confined well in the fibre and hence the output can be flexibly delivered to desired elements or targets. Most fibre lasers have a broad gain bandwidth, making it possible to tune the output wavelength and open up the way for ultrashort pulse generation. The absorption band of doped fibres is broad too. This makes the exact pump wavelength a non-critical issue. The beam quality of fibre lasers is high and usually diffraction-limited. Rare-earth doped fibres have very high gain efficiency, which enables the lasers to be operated with relatively low pump power. High gain efficiency also means that high power operation can be realized. More importantly, fibre lasers remove the strict requirement of heat management which is normally very critical in solid state lasers. Optical fibre has a high surface-to-volume ratio, so heat can be dissipated very efficiently through air-cooling. Ever since the first diode laser developed by Hall *et. al*. [3] in 1962, direct diode pumping for fibre lasers is at ease for fibre laser. Moreover, fibre lasers are alignment free as the gain medium – the fibre itself is a cylindrical waveguide that confines the light well in the medium. This causes a high overlapping factor for both the pump light and the laser light within the medium.

The first fibre laser, a neodymium-doped glass fibre laser pumped by a flashlight, operating in pulsed mode, was constructed and developed by Snitzer in 1961 [4]. The fibres were tested in different sizes (diameters). The cladding had a refractive index of 1.52. Stone *et. al*. [5] published a neodymium fibre laser pumped by a LED in 1976. It

was the first laser to be operated in continuous wave at room temperature with a single LED pump. It was also the first Nd glass laser operating without a heat sink.

2.2 *Q*-Switching of Laser

Laser with the output power being constant over time is known as continuous wave (CW). Many types of lasers can be made to operate in CW mode to satisfy such an application. Rather than CW emission, many applications require the emission be modulated or pulsed. These lasers are commonly referred to as pulsed lasers. Pulsed operation of laser is where the optical power appears in pulses of some duration at some repetition rate. In its simplest definition, optical pulses are flashes of light, which can be generated with lasers and delivered in the form of laser beams. Due to the very high frequencies, optical pulses can be extremely short (ultrashort) when their optical bandwidth spans a significant fraction of the mean frequency. Pulsed operation of a laser can be realized by many different physical mechanisms depending on pulse duration, energy and repetition rate. Some of the common methods are gain switching, cavity dumping, *Q*-switching and mode-locking. The two latter are the most common techniques for pulsing lasers. *Q*-switching typically produces energetic pulses in the nanosecond range and repetition rates of a few hertz to kilohertz. On the other hand, mode-locking technique produces shorter pulses with much higher repetition rates, typically with femtosecond to picosecond duration and tens of megahertz repetition rate. Mode-locked lasers are best suited to applications where extremely accurate material cutting or removal is required, for instance corneal surgery, photonic sampling, material deposition to form nanostructures and terahertz wave generation. Despite the fact that mode-locking is the most frequently used method for generating ultrashort pulses, the *Q*-switching approach remains a technique of great importance in many different laser systems. *Q*-switched lasers are useful in many applications such as material processing,

range finding, remote sensing, holography range finding, remote sensing, holography, nonlinear frequency conversion, nonlinear optics studies and many others.

2.2.1 Principle of *Q*-Switching

The result of *Q*-switching is a short, intense pulse of laser radiation – sometimes called a "giant pulse". *Q* refers to the "quality factor" of the laser resonator. The idea of *Q*-switching is a take-off of some well known techniques used in low frequency electronics for the generation and switching of high power. For instance, consider a simple technique for generating high peak pulsed power, as seen in Figure 2.1 below.

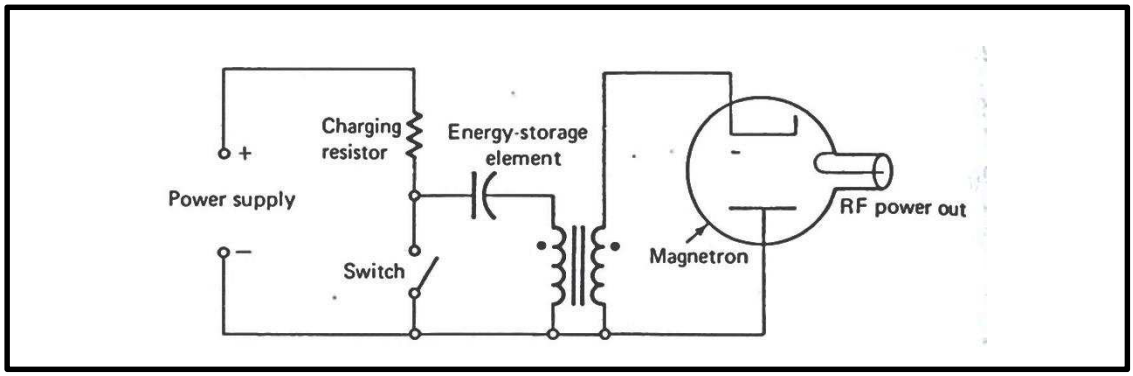

Figure 2.1: Schematic illustration of a simple electric circuit for generating high peak pulsed power. (reproduced from ref [6])

Energy is extracted from the primary source, the power supply, at a reasonable rate limited by the charging resistor to be P_{max} – the pumping cycle. The energy is stored by the capacitor, which is prevented from discharging by the open circuit of the switch. Once the switch is opened, the only thing limiting the capacitor discharge current is the impedance of the load – the power cycle. It should be clear that the peak power delivered to the load can be many times the peak instantaneous power extracted from the source.

These same ideas, utilized in the "giant pulse operation" of a laser, use the fact that energy can be stored for future use by creating a population inversion. Spontaneous emission out of the upper state represents a drain on the stored energy, much as would a leakage path on the capacitor.

Spontaneous emission causes a difficulty because it is amplified by the population inversion and will build up to a steady state value whose intensity is limited by the rate at which energy can be pumped into the system. To avoid this drain on the population inversion, the laser is prevented from oscillating by making the loss per pass very high while pumping the system. If amplified spontaneous emission can be prevented from saturating the active medium with a single pass gain length, then considerable energy can be stored in the population inversion difference. This stored energy can be extracted by suddenly lowering the loss. Under these circumstances, the gain greatly exceeds the loss and the intensity rapidly builds up from spontaneous noise, reaching a level where further growth is impossible.

In other words, *Q*-switching involves deliberately introducing a time-dependent loss into the cavity. With a high loss present, the gain due to the population inversion can reach quite large values without laser action occurring. The high loss prevents laser action while energy is being pumped into the excited state of the medium. When a large population inversion has been achieved, the cavity loss is suddenly reduced. Laser oscillations can then begin. The threshold gain is now much less than the actual gain and this ensures a very rapid build-up of laser oscillations. All the available energy is emitted in a single, large pulse. This quickly depopulates the upper lasing level to such an extent that the gain is reduced below threshold and lasing action stops. *Q*-switching dramatically increases the peak power obtainable from lasers. The time variation of some of the laser parameters during *Q*-switching is shown schematically in Figure 2.2.

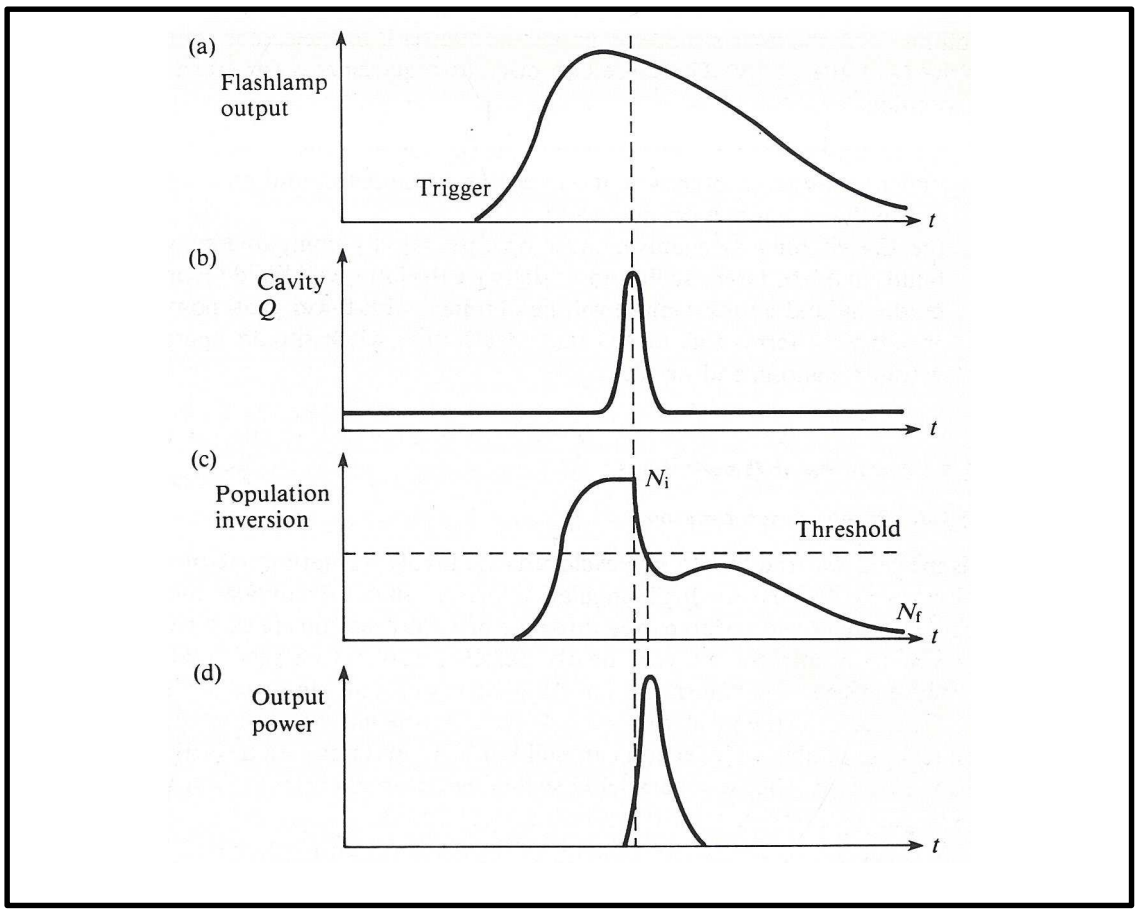

Figure 2.2: Variation of some laser parameters during *Q*-switching process. (a) Flashlamp output (b) Cavity *Q* (c) Population inversion (d) Output power as a function of time. (reproduced from ref [7])

Q-switching is actually also changing the *Q* value of the laser cavity. The *Q* value is inversely proportional to the energy dissipated per cycle. In a high loss situation therefore *Q* is small. When the loss is removed, *Q* 'switches' to higher values.

We may imagine *Q*-switching to be carried out by placing a closed shutter within the laser cavity, thereby isolating the cavity from the laser medium. After the laser has been pumped, the shutter is opened, restoring the *Q* of the cavity.

There are two requirements for effective *Q*-witching:

(1) the pumping rate must be faster than the spontaneous decay rate of the upper lasing level to build up a sufficiently large population inversion.

(2) the *Q*-switching mechanism must operate rapidly compared to the build-up of the laser oscillations.

Q may be defined as

$$Q = \frac{\text{resonant frequency}}{\text{laser linewidth}} \quad \text{..... (2.1) [7]}$$

This equation is not too helpful in calculating *Q*. Therefore, an alternative definition is needed, where

$$Q = \frac{2\pi \text{ x energy stored in the resonator at resonance}}{\text{energy dissipated per cycle.}} \quad \text{..... (2.2) [7]}$$

Consider a Fabry-Perot laser resonator, where bunch of photons, N_p, are travelling backwards and forwards between the resonator mirrors, as illustrated in Figure 2.3.

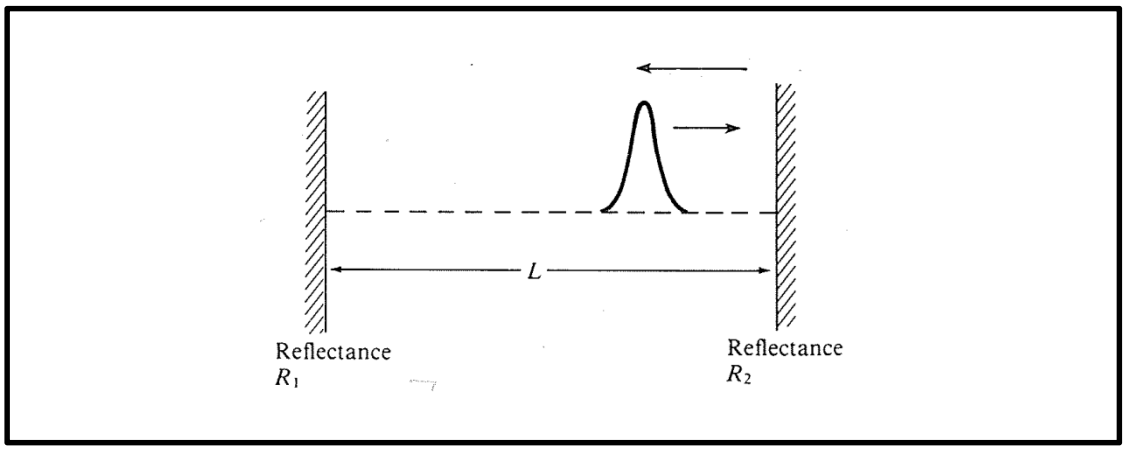

Figure 2.3: Photons bouncing back and forth between the mirrors in a laser cavity. (reproduced from ref [7])

After the photons have completed one round trip, their numbers will be reduce to $N_pR_1R_2$, where R_1 and R_2 are the mirror reflectances and the corresponding energy loss is $N_p\,(1 - R_1R_2)\,hv$, assuming no absorption losses in the mirrors. This loss occurs over a

time of $2L/c$ and hence the rate of energy loss is $N_p\ (1 - R_1R_2)hvc/2L$. Now the time taken for one cycle of the electric field of the corresponding electromagnetic wave is $1/v$ or λ/c and in this time the energy lost is $N_p\ (1 - R_1R_2)\ hv\lambda/2L$. The total energy in the cavity is $N_p hv$ and therefore the expression for Q can be written as

$$Q = \frac{2\pi N_p hv}{N_p hv\ (1-R_1R_2)\lambda/2L} = \frac{4\pi L}{\lambda}\frac{1}{(1-R_1R_2)} \quad \ldots\ldots (2.3)$$

2.2.2 Active *Q*-Switching

Q-switching can be realized with active or passive means. Active *Q*-switching is normally achieved by external modulation. Typical components for active *Q*-switching are rotating mirrors, electro-optic and acousto-optic modulators.

The most direct method is simply to mount one end mirror of the laser on a rapidly spinning motor shaft, so that the laser can only oscillate during the brief interval when the mirror rotates through an aligned orientation with respect to the opposite mirror. This method was the first to be developed. Optical losses will be large except for the brief interval during each rotation when the mirrors are nearly very parallel. Just before this point is reached, a mechanism triggers the pumping. As the mirrors are not quite parallel, the population inversion can build up without laser action starting. When the mirrors become parallel, *Q*-switching occurs and the *Q*-switched pulse then develops. The mirror rotation speeds involved may be as high as 1000 rev s^{-1}. This implies that the resonator could be *Q*-switched every 10^{-3} s.

Though cheap and simple, rotating mirror has some disadvantages. Even with the highest speed motors, this method suffers from uncertain timing, slow switching speed, lack of reliability, and vibration and mechanical noise which lead to alignment difficulties in the direction perpendicular to the plane of rotation. It is also quite impossible to *Q*-switched the resonator within microsecond range between the pulses because of the excessive heating which would occur in the laser resonator. Nonetheless,

this method is still useful on very long laser resonators at very long wavelengths, where mirror alignment is less critical.

In the electro-optic *Q*-switching method, one of the most useful no-mechanical switching techniques that may be used is based on the Pockels Effects. This effect concerns the behaviour of polarized light as it passes through certain electro-optic materials which are subject to electric fields. An electro-optic modulator consists of an electro-optic crystal which becomes birefringent under the influence of an applied electric potential difference, plus one or more prisms or other polarizing elements inside the laser resonator. An applied potential difference sufficient to make the Pockels crystal into a quarter wave plate is initially applied. Energy circulating once around the laser resonator has its polarization rotated by 90^o about the resonator axis so that all the circulating energy is coupled out of the cavity by the polarizing element after just one round trip. Switching the resonator to low loss condition is then achieved by suddenly turning this potential difference off. As an alternative, a fixed quarter wave element can create the high loss condition with no potential difference applied, and the Pockels crystal can then be switched on to cancel this birefringence.

Consider light emerging from the lasing medium. It will pass through the polarizer and hence become plane polarized. It then traverses the electro-optic crystal twice before returning to the polarizer. If the plane of polarization of the beam has been rotated through 90^o, it will be unable to pass through the polarizer, and the electro-optic crystal together with the polarizer that act as a shutter, will be effectively “closed”. With no potential difference applied, the shutter is “opened”. Therefore by switching the Potential difference and thereby the electric field to zero at the appropriate time, the laser can be *Q*-switched.

Electro-optic *Q*-switching provides the fastest for of *Q*-switching, with precise timing, good stability and repeatability, and a large hold-off ratio. However, this method requires expensive electro-optic crystal and a very fast high potential difference pulse source, typically at least several kilovolts in a few tens of nanoseconds. Nanosecond rise- time pulses at this potential difference level are difficult to obtain and can produce electrical interference in nearby electronic equipment. In addition, this method needs several elements inside the laser resonator. These elements may be optically lossy (the Pockels crystal in particular) and subject to optical damage at high intensities inside the *Q*-switched laser.

Acousto-optic effect is the change in the refractive index of a medium caused by the mechanical strains which accompany a acoustic wave as it travels through the medium. The strain, and hence the refractive index, will vary periodically with a wavelength equal to that of the acoustic wave. In effect, the acoustic wave sets up a diffraction grating which can then be used to deflect a light beam. If light in the visible region is being used, then fused silica is a suitable medium. Although an acoustic wave is being referred in this case, the frequencies used in practice are ultrasonic and way above the limit of human hearing. In Fig, when the acoustic wave is present, a significant fraction of the beam energy in the cavity is diffracted out of the cavity, thus introducing an additional loss mechanism and reducing the cavity *Q* value. When the acoustic wave is turned off, diffraction ceases and the *Q* value returns to its former high level.

Acousto-optic *Q*-switching has the advantages of very low optical insertion loss, relatively simple acoustic wave drive circuitry and ease of use for repetitive *Q*-switching at kHz repetition rates. The disadvantages would be they have only relatively slow opening times, as well as low hold-off ratios. They are primarily employed for lower gain CW pumped or repetitively *Q*-switched lasers.

2.2.3 Passive *Q*-Switching

Passive *Q*-switching uses some form of easily saturable absorbing medium inside the laser cavity. The effect comes about when the absorbing material is excited from the ground state to an excited state, reducing the ground state population. A saturable absorber (SA) is a material that has decreasing light absorption with increasing light intensity. SAs that show this effect are needed at the intensities typically found in solid-state laser cavities, and semiconductor SAs are ideally suited for this. The key parameters for a SA are

(i) the wavelength range (where it absorbs)

(ii) the dynamic response (how fast it recovers)

(iii) the saturation intensity and fluence (at what intensity or pulse energy density it saturates)

In SAs, the molecules absorb radiation so strongly that appreciable number of molecules can be excited to the upper level. If the ground state and excited state populations are almost equal, the absorption becomes very small. In such a case, the material is said to be “saturated”. Laser inversion is built up by the pumping process until the gain inside the cavity exceeds this absorption and laser oscillations begin to develop inside the cavity.

Consider placing such an absorber inside the cavity of a laser system. Initially, at low light levels, the absorber is “opaque”, thereby preventing laser action and allowing a large build-up of population inversion. As the light intensity builds up within the cavity, more and more of the absorber’s excited states become populated. This leads to an increase in intensity. In a very short time, the oscillation at some relatively low level then rapidly saturates the absorber and thus opens up the cavity, leading to the development of a rapid and intense giant pulse.

In general, the advantages of active *Q*-switching over passive are the controllable repetition rate and low timing jitter. Fundamentally, timing jitter in a *Q*-switched laser is inevitable because the first photon of the oscillation modes comes from spontaneous emission of the gain medium. Usually, in actively *Q*-switched lasers, the pulse width decreases and pulse energy increases with increasing pump power. The pulse width in actively *Q*-switched lasers has the following dependence on the gain and cavity round trip gain coefficient:

$$\tau_p = 8.1 \text{ x } t_{rt}/g_{rt} \ldots\ldots (2.4)$$

where t_{rt} is the cavity round trip time and $g_{rt} = \ln G_{rt}$ is the round trip gain coefficient when the pulse begins to form. From the expression, one can easily see that shortening the cavity length shortens the pulses and heavier pumping also reduces the pulse width. In active *Q*-switching, the pulse energy can be increased to certain limit by reducing the repetition rate. This divides the gain to fewer pulses, so individual pulses receive higher gain. When the pulse cycle time exceeds the gain material upper state lifetime, the amplified spontaneous emission starts to limit the pulse energy.

Passive *Q*-switching is generally simple, convenient, more cost effective, more compact, and requires minimum of optical elements inside the laser and no external driving circulatory and hence less control of cavity parameters. Usually the pulse width and pulse energy are quite independent of the pump power. The repetition rate is linearly proportional to the pump power. One setback of passively *Q*-switched lasers is the timing jitter – fluctuation in the timing of the pulses in the pulse train. In addition, the saturable absorber (SA) used may need careful initial adjustment and may be subject to chemical and photochemical degradation in use.

2.3 Theoretical Model of *Q*-Switching

Theoretical models describing *Q*-switching of lasers are broadly covered in various text books [8, 9]. In this section, the pulse energy, pulse width and repetition rate of a pulsed laser *Q*-switched by SA is reviewed briefly.

2.3.1 Pulse Energy

The expression for pulse energy can be written as

$$E_p = E_L \Delta g \ \frac{l_{out}}{l_{out+}\, l_p} \leq E_L g_i \ldots\ldots (2.5)$$

Where E_L is the saturation energy of the laser gain medium, $\Delta g = g_i - g_f$ is the gain reduction by *Q*-switched pulse. g_i and g_f are the intensity gain coefficients just before and after the pulse. l_{out} is the output coupling coefficient and l_p is the parasitic loss coefficient, dominated by the non-saturable loss of the SA.

The pulse cycle can be divided into four phases, as seen in Figure 2.4. In the beginning, the SA is in its non-saturated state. The pulse starts to evolve when the gain has reached the level of the unsaturated value of the losses

$$g_i = l + qo \ldots\ldots (2.6)$$

where $l = l_{out} + l_p$ and q_o is the non-saturated loss coefficient (the SA in its initial state) q_o is proportional to the modulation depth ΔR of the SA. The modulation depth is defined as the difference of the high and low intensity state reflectivities. The intracavity power *P* starts to grow until the intensity is sufficient to saturate the absorber. The saturation energy of the SA is typically chosen to be at least 1 order of magnitude less than the pulse energy, so the absorber is saturated well before *P* reaches its maximum. Moreover-, the absorber recovery time $\tau_{rec} \geq \tau_p$, so the absorber has only a minor influence on pulse development at latter phases.

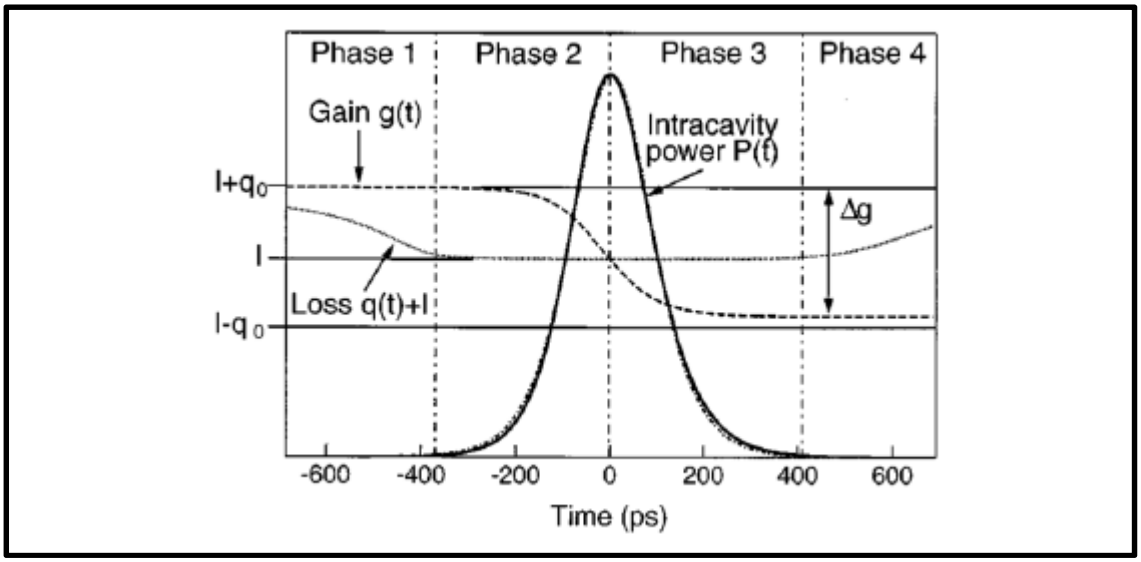

Figure 2.4: Evolution of power, loss and gain on the time scale of the pulse width. The peak of the *Q*-switched pulse is reached when the gain equals the total losses.

In phase 2, the SA is fully saturated. The net gain is $g = g_i - l - q \approx q_o$, since the saturable loss coefficient $q = 0$ when the absorption is completely saturated. The pulse maximum is reached when the net gain is zero ($g = l$). In phase 3, the net gain is negative and the intracavity power decreases. In phase 4, the SA has already recovered from the saturation and the pumping of the gain to the threshold level takes place. The SA recovery time is much shorter than the gain recovery, so the absorber is fully recovered when phase 1 starts a new cycle.

The gain reduction Δg depends on q_o and l. In most practical cases, the laser is operated in the regime where $q_o \approx l$, at which point the pulse energy is optimized and the pulse shape is nearly symmetrical. If $l \geq q_o$, the assumption $\Delta g = 2qo$ is valid. Inserting Δg into Equation (), we obtain the expression for pulse energy to be

$$E_p \approx E_L 2q_o \frac{l_{out}}{l_{out} + l_p} = \frac{h\nu_L}{2\sigma_L} A 2q_o \frac{l_{out}}{l_{out} + l_p} \text{ ….. (2.7)}$$

where $q_o \leq 1$.

In the latter expression, the saturation energy E_L is expanded. In the latter form $h\nu_L$ is the photon energy, σ_L is the emission cross section of the laser material, and A is the mode area. We can increase the pulse energy by increasing the non-saturated loss q_o and l up to the limit set by the available gain $g_i = l + q_o$. Moreover, we have to take into account the parasitic loss l_p. When realizing pulsing with SESAMs, increasing the modulation depth usually increases the non-saturable loss ($\Delta R \approx q_o$ and $\alpha_{ns} \approx l_p$). It has been shown in () that when there is some parasitic loss preset, the pulse energy is optimized when the combined loss l is close to the unsaturated value of loss q_o, that is $l \approx q_o$.

2.3.2 Pulse Width

The expression for pulse width can be formulated as follows: we can assume that the saturation energy of the absorber is small compared to the pulse energy, and thus phase 1 in Fig has only little influence on the full width at half maximum (FWHM) of the pulse. We can further assume that in the beginning of phase 2, the gain is depleted [$g(t) = g_i$], but the absorber is fully saturated [$q(t) = 0$]. The net gain is thus $g_i - l - q \approx q_o$. In phase 3, the net gain is $g_f - l - q = -\Delta g + g_i - l - q \approx q_o$, since the absorber is still fully saturated ($q = 0$). This results in the growth rate and the decay rate of the Q-switched pulse both being q_o/t_{rt}, where t_{rt} is the cavity round trip time. This leads to an estimated FWHM pulse width of $\tau_p \approx 2\ln 2 t_{rt}/q_o$. Taking into account the decrease in growth and decay of the pulse during saturation of the gain widens the pulse by another factor of ~2, and results the expression to be the following [10, 11]:

$$\tau_p = \frac{3.52\, t_{rt}}{q_o} \quad \text{….. (2.8)}$$

It should be noted that this expression gives the lower limit for pulse length achievable using a passively Q-switched laser. The pulse width of a practical laser setup might be somewhat longer due to non-ideal components. However, the formula indicates clearly

that to shorten the pulse we need to shorten the cavity round trip time and increase the non-saturated loss, which in practical terms means increasing the modulation depth of the SA being used.

2.3.3 Repetition Rate

The repetition rate can be calculated by dividing the average output power by the pulse energy. From [10], the average power is

$$P_{av} = \eta_s (P_p - P_{P,th}) \text{ ….. } (2.9)$$

where η_s is the slope efficiency and P_P and $P_{P,th}$ are the pump power and threshold pump power respectively. The repetition rate is thus

$$f_{rep} = \frac{\eta_s (P_p - P_{P,th})}{E_p} \alpha \text{ r} - 1 \text{ ….. } (2.10)$$

Here $r = \frac{P_p}{P_{pth}}$ is the pump parameter. We can further connect the pump powers to the small signal gain coefficient g_o and the loss the coefficients by expressing them as

$$P_P = \frac{h\nu_p A}{2\sigma_L \tau_L \eta_p} g_o, \qquad P_{P,th} = \frac{h\nu_p A}{2\sigma_L \tau_L \eta_p} (l + q_o) \text{ ….. } (2.11)$$

In these expressions, $h\nu_p$ is the pump photon energy, α_p is the pumping efficiency and τ_L is the upper state lifetime of the gain medium. Inserting the equation of pulse energy ($E_p = E_L \Delta g \frac{l_{out}}{l_{out} + l_p}$) and pump power ($P_{P,th} = \frac{h\nu_p A}{2\sigma_L \tau_L \eta_p} (l + q_o)$) into $f_{rep} = \frac{\eta_s (P_p - P_{P,th})}{E_p}$ gives the expression for repetition rate as follows:

$$f_{rep} \approx \frac{g_o - (l + q_o)}{\Delta g \tau_L} \approx \frac{g_o - (l + q_o)}{2 q_o \tau_L} \text{ ….. } (2.12)$$

The expression can be further simplified when operating far above the threshold by neglecting the term $l + q_o$:

$$f_{rep} \approx \frac{g_o}{2 q_o \tau_L} \text{ ….. } (2.13)$$

Because $g_o >> L + q_o$ when operating well above threshold.

The formulas derived show the basic relations between the laser output characteristic and operation parameters.

2.4 Semiconductor Saturable Absorber Mirrors

SAs used in the past were typically dyes, which have short lifetimes, high toxicity and complicated handling procedures. Alternative solid-state SAs include crystals such as Cr:YAG, which typically operate for only a limited range of wavelengths, recovery times and saturation levels. Semiconductor materials, however, can absorb over a broad range of wavelengths, from visible to the mid-infrared. The absorption recovery time and saturation fluence can be controlled by altering the growth parameters and device design.

Semiconductor saturable absorber mirrors (SESAMs) are SAs that integrated into a mirror structure, resulting in a device that reflects more light the more intense the light is. SESAM operates in reflection geometry and thus the reflectivity increases with higher incoming pulses. SESAM can operate in transmission mode as well. SESAM has designs that can cover wavelengths from less than 800 nm to more than 1600 nm, pulse widths from femtoseconds to nanoseconds and power levels from milliwatts to more than 100 watts.

Saturation absorption is a property of materials where the absorption of light decreases with increasing light intensity. A semiconductor absorbs light when the photon energy is sufficient to excite carriers from the valence band to the conduction band. Under conditions of strong excitation, the absorption is saturated because possible initial states of the pump transition are depleted while the final states are partially occupied. Within 60 - 300 fs of excitation, the carriers in each band thermalize, and this leads to a partial

recovery of the absorption. On a longer time scale, typically between a few picoseconds and a few nanoseconds, the carrier will be removed by recombination and trapping.

The absorption process can also be thought of in terms of excitation levels: an electron at the valence band gets excited by the incident photons and is lifted to the conduction band. The amount of absorption can be described by the absorption coefficient α, which describes the population at the excited and ground levels. When the excitation process is repeated at a sufficiently high pace, i.e. the intensity of the incident photons is high enough compared to the relaxation of the excitation, the valence band gets depleted, and the amount of absorption decreases. In other terms, the absorption becomes bleached or saturated at high intensities. In a two-level system, the absorption can be described by the equation

$$\alpha = \frac{\alpha_0}{1+I/I_S} \quad \ldots\ldots (2.14)$$

where α_o is the low intensity absorption coefficient, I the intensity and I_s the saturation intensity.

The smaller the emission cross-section, the stronger the tendency for self-*Q*-switching. This means that the parameters of the SA have to be carefully adapted to prevent *Q*-switching instabilities. SAs with the parameters, such as modulation depth, saturation fluence and non-saturable losses, required for a given laser cavity and pump power are obtained using semiconductor mirror devices. Different semiconductor materials provide a wide range of band gaps for operation from the visible to the far-infrared spectral range. Therefore, band gap engineering can provide broad tunability. In addition, defect engineering for recovery times ranging from the nanosecond to the femtosecond regime is possible. SAs can be adjusted to the required absorber parameter even when the mode size is fixed. Typically, the SESAM is operated with an incident pulse fluence of about three to five times that of the saturation fluence. This saturation

level of the absorber provides nearly the maximum modulation depth without damaging the device [12]. Higher saturation also reduces the tendency for *Q*-switching instabilities because of thermal effects and two-photon absorption, which becomes more significant for femtosecond pulses. The recovery time of the SESAM can be as long as 10 to 30 times relative to the final pulse duration [12].

SESAM design depends strongly on the laser parameters and can be optimized for different operational regimes.

A SA may also produce *Q*-switched mode-locking, where the laser emits bunches of mode-locked pulses, which may or may not have a stable *Q*-switching envelope. *Q*-switching instabilities occur when the pulse energy is temporarily increased because of noise fluctuations in the laser, which then gets even further increased because of the stronger saturation of the SA. This has to be balanced by a stronger saturation of the gain. If the gain is not sufficiently saturated then the pulse energy will increase further and self- *Q*-switching occurs. The physical background of *Q*-switching instabilities can be summarized by a simple guideline: *Q*-switching instabilities in ion-doped solid-state lasers can be prevented if $E_p^2 > E_{sat,L} E_{sat,A} \Delta R$, assuming that the SA is fully saturated.

The important parameters are:

(i) the intracavity energy, E_p,

(ii) the intracavity average power, P_{intra},

(iii) the pulse repetition rate, f_{rep},

(iv) the saturation energy of the laser medium, $E_{sat,L}$,

(v) the average mode area inside the laser medium, $A_{eff,L}$,

(vi) the emission cross-section of the laser gain medium, $\sigma_{em,L}$,

(vii) the saturation energy of the absorber, $E_{sat,\,A}$,

(viii) the average mode area inside the SA, $A_{eff,A}$,

(ix) the saturation fluence of the SA, $F_{sat,A}$,

(x) the modulation depth of the SA, ΔR.

2.5 The Chemical Structure of Graphene Oxide

There is no unambiguous model exists for the precise chemical structure of GO. The main reasons are the complexity of the material due to its amorphous, berthollide character and the lack of precise analytical techniques for characterizing such materials. Many of the earliest structural models of GO proposed regular lattices composed of discrete repeat units. Figure 2.5 shows Hofmann's structure consisted of epoxy groups spread across the basal planes of graphite, with a net molecular formula of C_2O [13].

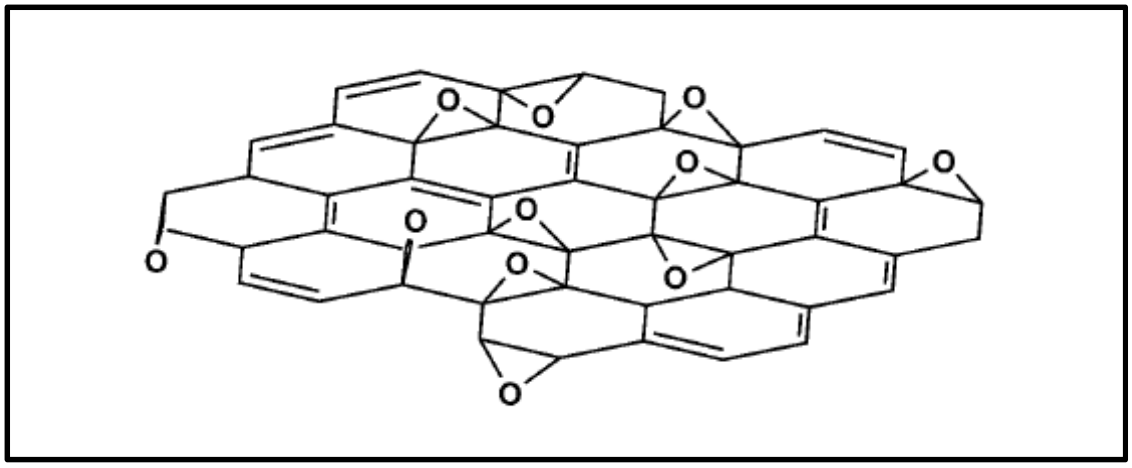

Figure 2.5: Hofmann's proposed structure of graphene oxide. (reproduced from ref [14])

A variation of this model was proposed by Ruess in 1946 [15] which incorporated hydroxyl groups into the basal plane, accounting for the hydrogen content of GO. This model also altered the basal plane structure to a sp^3 hybridized system rather than the sp^2 hybridized model of Hofmann. Ruess's model assumed a repeat unit as well, as seen in Figure 2.6 below.

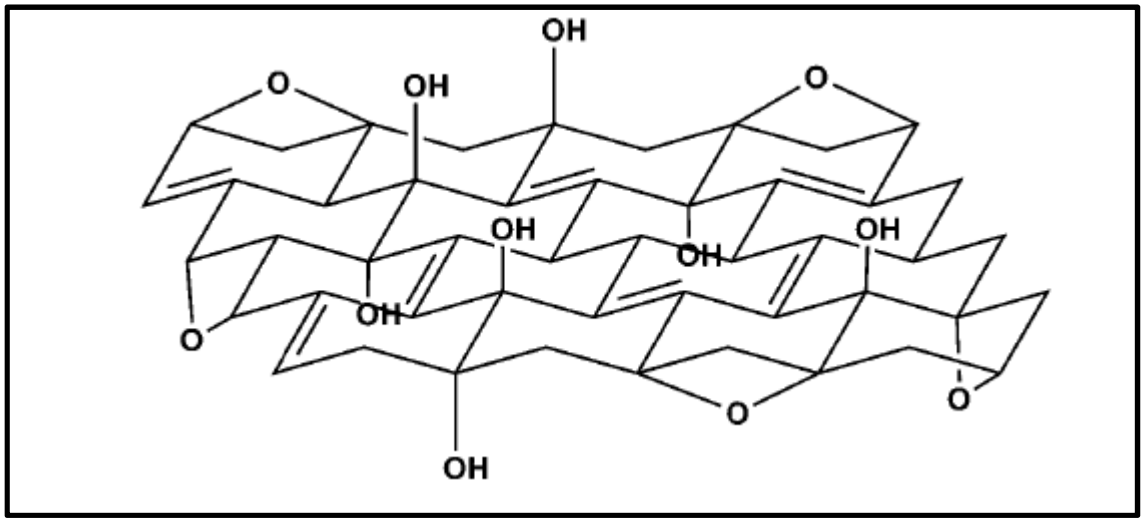

Figure 2.6: Ruess's model of GO chemical structure, with hydroxyl groups in the basal plane. (reproduced from ref [14])

In 1969, Scholz and Boehm suggested a model that completely removed the epoxide and ether groups, substituting regular quinoidal species in a corrugated backbone [16], as seen in Figure 2.7 below.

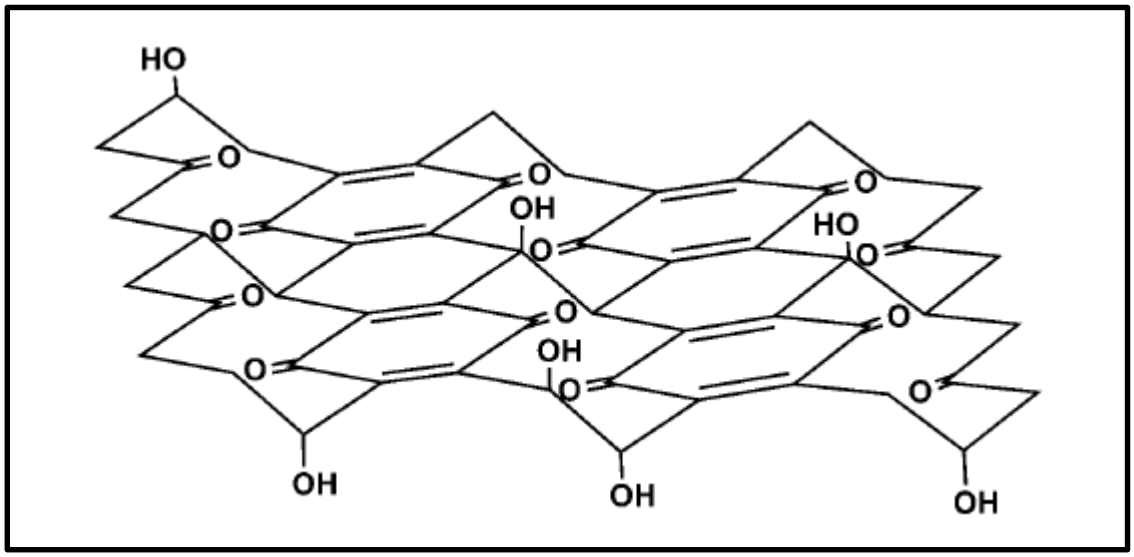

Figure 2.7: Scholz and Boehm's model with quinoidal species. (reproduced from ref [14])

Another remarkable model by Nakajima and Matsuo relied on the assumption of a lattice framework akin to poly(dicarbonmonofluoride), $(C_2F)n$, which forms a stage 2 graphite intercalation compound (GIC) [17]. They have made a valuable contribution to understanding the chemical nature of GO by proposing a stepwise mechanism for its formation via 3 of the more common oxidation protocols [18]. This is shown in Figure 2.8

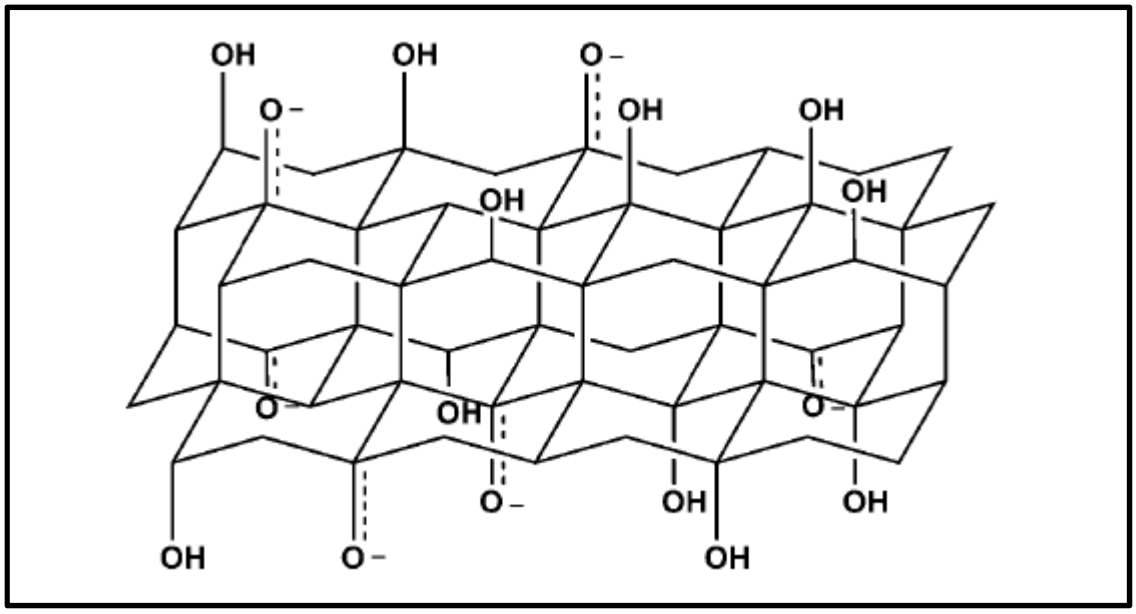

Figure 2.8: Nakajima and Matsuo's model of GO, incorporating a lattice framework related to poly(dicarbonmonofluoride), forming a stage 2 graphite intercalation compound. (reproduced from ref [14])

The model proposed by Lerf and Klinowski [19] is the most well-known and widely cited in most contemporary literatures. This model is shown in Figure 2.9. Initially, solid state nuclear magnetic resonance (NMR) spectroscopy was used to characterize the material [20]. Subsequently, Lerf and co-workers were also able to isolate structural features based on the material's reactivity [21]. It was shown that all carbons in GO are quaternary, based on Mermoux's model [22]. Short-contact time experiments also showed that there was significant interplatelet hydrogen bonding through the alcohols and epoxide functional groups, contributing significantly to the stacked structure of GO.

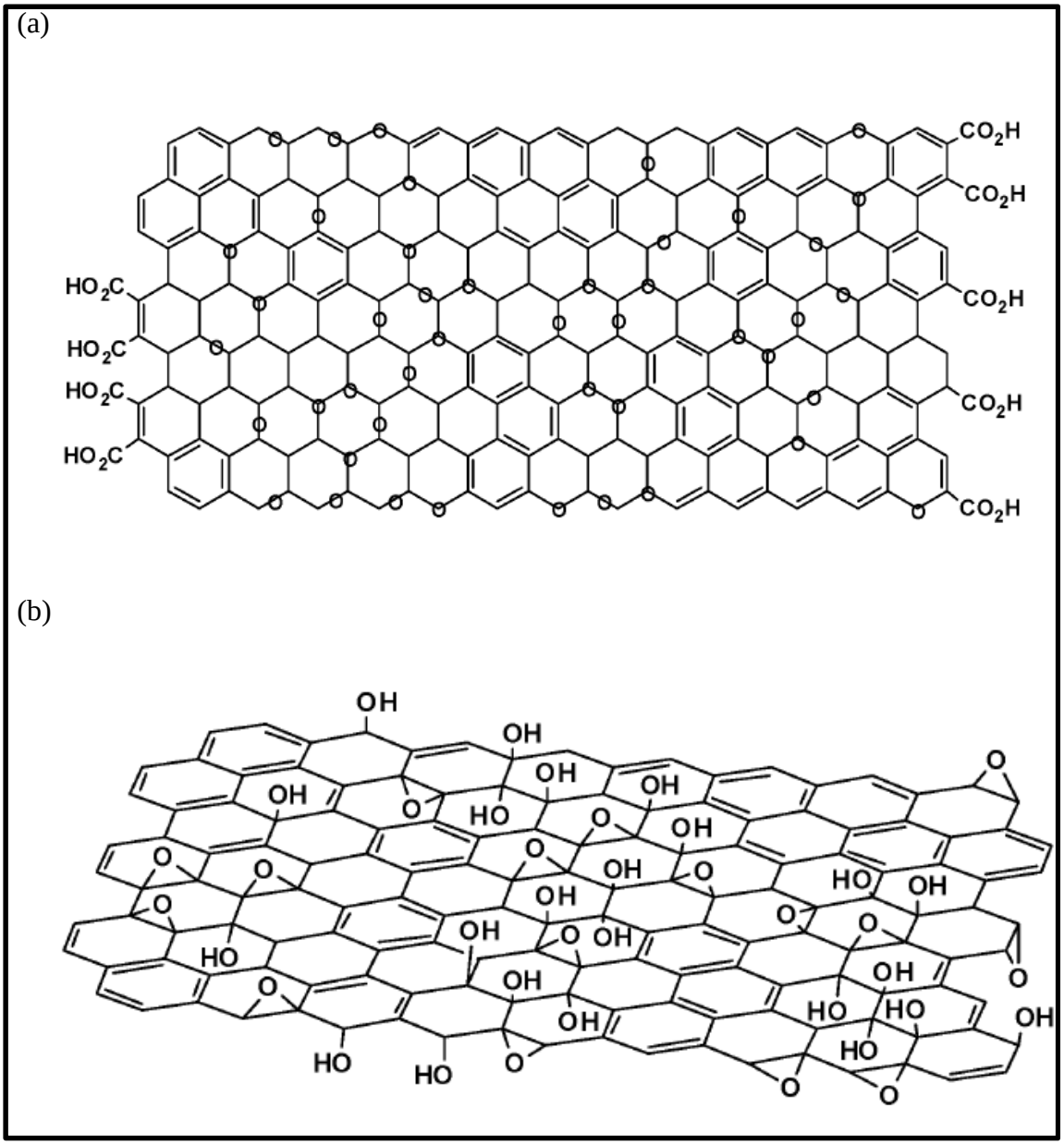

Figure 2.9: Lerf and Klinowski proposed structure of GO with (a) the presence (b) the absence of carboxylic acids on the periphery of the basal plane of the graphitic platelets of GO. (reproduced from ref [14])

Treatment of GO with D_2O eliminated the water peak in the respective ^1H NMR spectrum, allowing for resolution of proton signals buried beneath the intense resonance caused by water bound to the surface of GO. The signal attributed to the tertiary alcohols was not significantly affected, indicating a slower exchange process, relative to the water molecules intercalated into the interlayer of GO. A second peak was observed, indicative of the presence of at least two magnetically inequivalent alcohol species. It is

reasonable to surmise that it is reflective of strong hydrogen bonding interactions either to water intercalated between the platelets or to other platelets. These results indicate that the dominant structural features present on the surface of GO are tertiary alcohols and ethers and have been the basis for a variety of reactivity studies.

In the NMR studies, the full-width-half-maximum height of the water peak remains nearly constant across a wide temperature, indicating very strong interactions between the water and the GO [23]. This is likely a key factor in maintaining the stacked structure of GO. It has been confirmed through neutron scattering that the water is strongly bound to the basal plane of GO through hydrogen bonding interactions with the oxygen on the epoxides of the GO [24-26]. By reacting GO with arrange of reactive species, Lerf and co-workers determined that the double bonds were likely either aromatic or conjugated [21]. The reason being is that isolated double bonds would be unlikely to persist in the strong oxidizing conditions used. The revised model also indicates that carboxylic acid groups were present in very low quantities at the periphery of the graphitic platelets [16].

Though the Lerf-Klinowski model remains largely unchanged, others have made slight modifications to the proposed structure including the presence of 5- and 6-membered lactols on the periphery of tertiary alcohols on the surface, though all accounts maintain the dominance of epoxides and alcohols on the basal plane [27, 28]. Cai *et. al.* have demonstrated the ability to isotopically label GO, greatly expanding the scope of potential spectroscopic techniques that may be applied to the study of its structure [27]. One notable exception to this adherence to the Lerf-Klinowski model has been proposed by Dékány (Figure 2.10.) [29]. The Dékány model work revised and updated the Ruess and Scholz-Boehm models, which suggested a regular, corrugated quinoidal structure interrupted by *trans*-linked cyclohexyl regions, functionalized by tertiary alcohols and 1,3-ethers. No carboxylic acids are believed to be present in this description of GO.

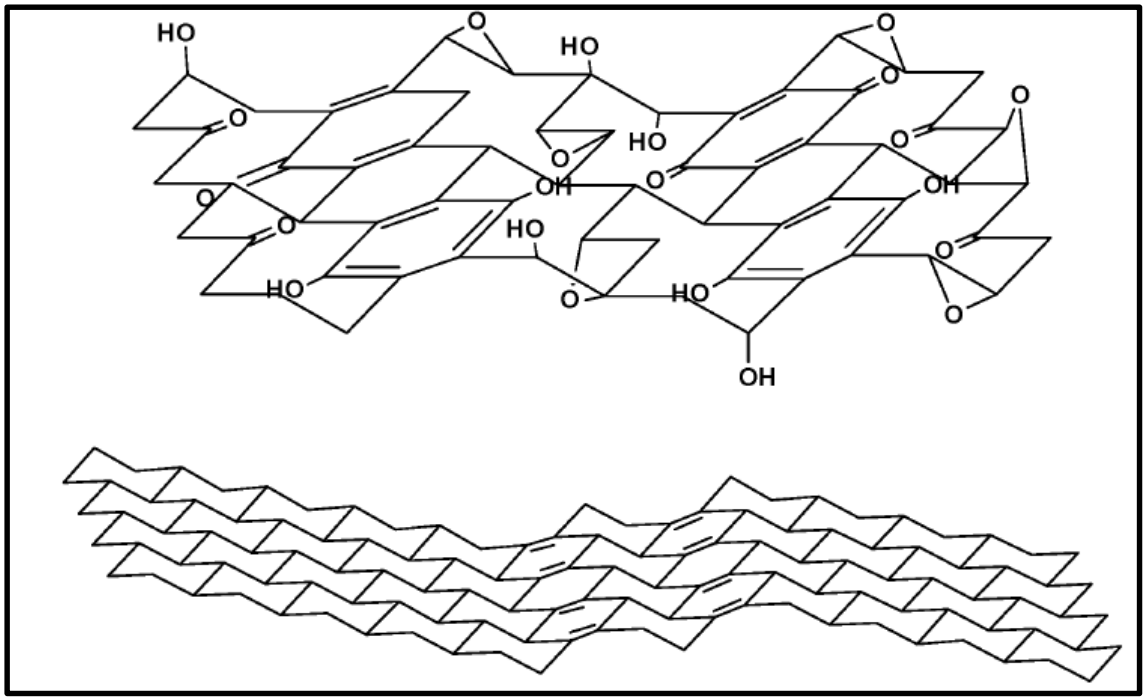

Figure 2.10: GO structure as proposed by Dékány and team. (reproduced from ref [14])

In summary, variations in the degree of oxidation caused by differences in starting materials or oxidation protocol can cause substantial variation in the structure and properties of the material. It is predicted that partial oxidation is thermodynamically favoured over complete oxidation [30]. Nonetheless, the exact identity and distribution of oxide functional groups depends strongly on the extend of coverage. This is illustrated in the theoretical prediction that the ratio of epoxides to alcohols increases with increasing oxidation [30].

2.6 Saturable Absorption Properties of Graphene Oxide

The optical and saturable absorption properties of GO can be understood first from that of graphene's. The optical conductance of monolayer graphene is defined solely by the fine structure constant, $\alpha = e^2/\hbar c$ (where e is the electron charge, $\hbar$ is Dirac's constant and c is the speed of light). The absorbance has been predicted to be independent of frequency. In principle, the interband optical absorption in zero-gap graphene could be saturated readily under strong excitation due to Pauli blocking. The electronic and optical properties of graphene can be described in terms of massless Dirac fermions with linear dispersion near the Fermi energy. The optical interband transitions are expected to be frequency independent and solely determined by the optical conductance in a broad range of photon energies. The large absorption of atomic-layer graphene implies lower saturation intensity or higher photocarrier density compared to traditional semiconductor materials. It has been calculated that a single graphene sheet can absorb a significant fraction ($\pi\alpha$ = 2.3%) of incident infrared-to-visible light [31-35]. Therefore, in principle, graphene can be saturated readily under strong excitation from visible to near-infrared region due to the universal optical absorption and zero band gap. Figure 2.11a shows excitation processes responsible for absorption of light in monolayer graphene, in which electrons from the valence band (orange) are excited into the conduction band (yellow). Shortly after photo-excitation, these hot electrons thermalize and cool down to form a hot Fermi-Dirac distribution (Figure 2.11b) with electronic temperature T_e [8,9]. These newly created electron-hole pairs could block some of the originally possible interband optical transitions in a range of $k_B T_e$ (k_B is the Boltzmann constant) around the Fermi energy E_F and decrease the absorption of photons $\hbar\omega \approx k_B T_e$. In the following ~ 1 picosecond, intraband phonon scattering further cools the thermalized carriers. After that, electron-hole recombination will dominate the process until the equilibrium electron and hole distribution is restored, as shown in Figure 2.11b

[36, 37]. However, these only describe the linear optical transition under low excitation intensity. As the excitation is increased to higher intensity, the photogenerated carriers increase in concentration and cause the states near the edge of the conduction and valence bands to fill, blocking further absorption (Figure 2.11c) and thus imparting transparency to light at photon energies just above the band edge. Band filling occurs because no two electrons can fill the same state. Thus, saturable absorption is achieved due to this Pauli blocking process [38].

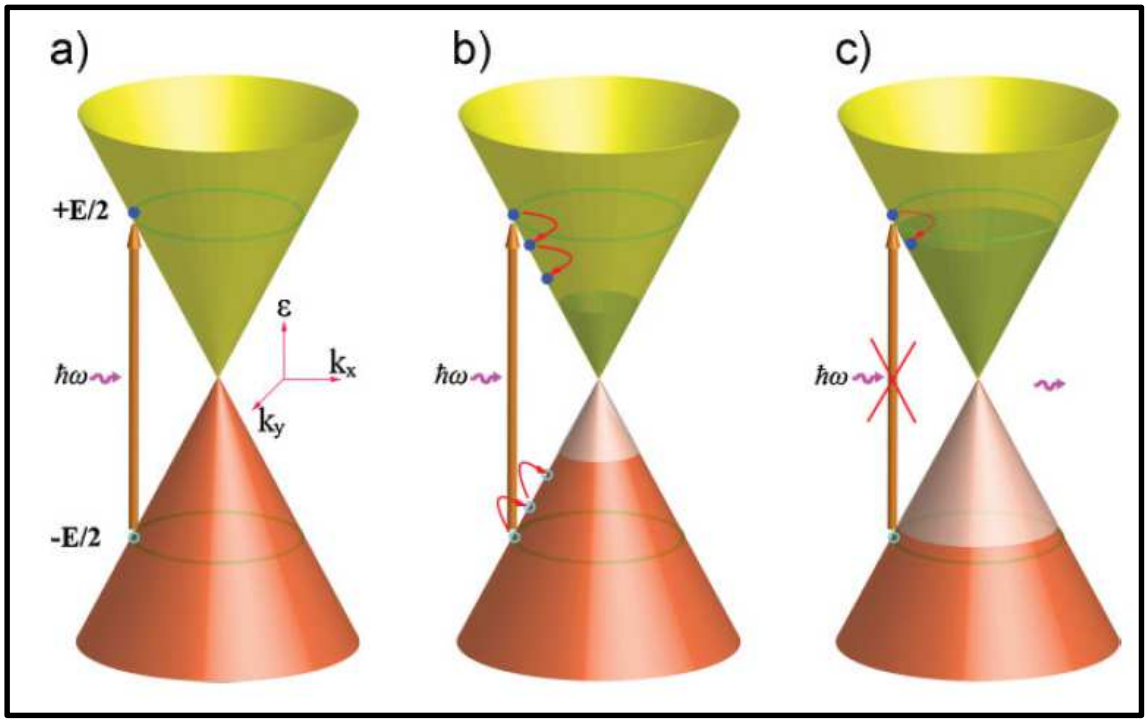

Figure 2.11: The process of saturable absorption. a) Optical interband transition via absorption of photon. b) The photogenerated carriers cool down to form a Fermi-Dirac distribution. Electron-hole equilibrium is achieved via intraband phonon scattering and electron-hole recombination. c) At high intensities, the photogenerated carriers cause the states near the edge of the conduction and valence bands to be filled and saturated, blocking further absorption. (reproduced from ref [39])

As for GO, the structure is unique in that the graphene basal plane is retained. An ideal graphene consists entirely of sp^2 hybridized carbon atoms. By contrasts, GO is a two-dimensional network consisting of variable sp^2 and sp^3 hybridized carbon atoms. GO is a covalent material with majority of the carbon atoms in the basal plane being sp^3 hybridized through σ-bonding with oxygen in the form of epoxy and hydroxyl groups.

Carbon atoms bonded with oxygen groups are sp^3 hybridized and disrupt the sp^2 conjugation of the hexagonal graphene lattice in GO – sp^3 carbon sites act as large repulsive barriers for carriers [40] and thus destroy the linear dispersion of the Dirac electrons and influence the unique optical properties of graphene. This will make GO unsuitable as a broadband saturable absorber pulsed lasers generation. Nonetheless, it has been shown, that GO, similar to graphene, also exhibits saturable absorption [41].

2.7 Review of Development of Graphene Oxide Based *Q*-Switched Fibre Lasers

Since the first demonstration of graphene based *Q*-switched fibre laser [42], extensive research has been carried out in the use of its precursor – graphene oxide as a passive SA material for *Q*-switching. There has been significant work in the demonstration of GO based *Q*-switched fibre lasers. In this section, the development of GO based *Q*-switched lasers is briefly reviewed and the performance is summarized.

Several types of SA device structures have been realized. Optical deposition of GO solution onto fibre end ferrule is one of the most common methods [43, 44]. More recently, SA device structure based on evanescent field interaction between optical mode and GO solution is also demonstrated [45]. The method enables GO to be deposited on a tapered fibre with waist diameter ~6.5 μm and waist length ~5 mm. It has a insertion loss of 1.5dB. In another work, GO suspension is sprayed onto the flat face of a *D*-shaped fibre [46]. Other than that, GO film based device structure has been proposed and successfully demonstrated [47, 48]. Some authors have shown that GO composite film such as chromium, gold and polyvinyl alcohol (PVA) can be used to generate *Q*-switched pulses as well [49-51].

On performance, Zhao *et. al*. has used GO for *Q*-switching of an erbium-doped fibre laser (EDFL), obtaining 2.72 μs pulses at five wavelengths operation [51]. Ahmad *et. al*. also demonstrated a GO *Q*-switched EDFL [44]. The narrowest pulse achieved has

duration of 6.6 μs at a repetition rate of 61 kHz. On a special note, a *Q*-switched mode-locked (QML) fibre laser was demonstrated, having a *Q*-switched envelope of ~2.63 μs temporal width and ~71.3 kHz repetition rate [46]. The operating regime can be readily changed between mode-locking, *Q* switched mode-locked and *Q*-switching by just simply changing the polarization state of the oscillating light in the laser resonator.

Other than using erbium-doped fibre (EDF) as the laser gain medium, other gain media have also been used, such as thulium and ytterbium. Ref [43] reported a *Q*-switched thulium-doped fibre laser (TDFL) using GO as the SA in a ring laser configuration and obtained maximum repetition rate, average output power and pulse energy of 16.0 kHz, 0.3 mW and 18.8 nJ respectively, all at a pump power of 164 mW. The narrowest pulse duration is 9.8 μs. Another TDFL has been demonstrated as well [52], whereby a very high average output power i.e. 302 mW and very high pulse energy i.e. 6.71 μJ are obtainable. In the other hand, a ytterbium-doped fibre can also be used as the gain medium to generate dark pulses and *Q*-switched pulses by using a GO-based composite as SA [47]. These operation regimes are realized for the first time in the 1 μm band.

In terms of wavelengths operations, a novel design of *Q*-switched dual-wavelength fibre laser with narrow channel spacing has been proposed and demonstrated [53]. The fibre laser is built around a 3 m long erbium doped fibre as the gain medium and a 10 cm long photonic crystal fibre (PCF) as the element to generate the dual-wavelength output, and GO as the SA to generate pulses. This GO-based fibre laser can generate pulses with a repetition rate and pulse-width of 31.0 kHz and 7.0 μs, respectively, as well as an average output power and pulse energy of 0.086 mW and 2.8 nJ, respectively at the maximum pump power of 72 mW. A wavelength spacing tunable, multiwavelength *Q*-switched mode-locked fibre laser in an EDF resonator, with GO deposited on tapered fibre has been demonstrated, in which the wavelength spacing could be tuned by pump

power [45]. The highest repetition rate and pulse width achieved are 37.3 kHz and 7.0 μs respectively when the laser is operating in the *Q*-switching regime.

Table 2.1 presents a selection of demonstrations of several types of GO-based *Q*-switched fibre lasers, SA device type and performance comparison.

Table 2.1: A list of reported GO-based *Q*-switched lasers and their respective performance.

Laser type	**SA device structure**	**Laser parameters**					
		Wavelength	**Pulse width**	**Maximum repetition rate**	**Maximum average output power**	**Maximum pulse energy**	**Ref.**
TDFL	Direct optical deposition	1942 nm	10 μs	16.0 kHz	0.3 mW	18.8 nJ	[43]
TDFL	Direct optical deposition on tapered fibre	2032 nm	3.8 μs	45.0 kHz	302 mW	6.71 μJ	[52]
EDFL	Direct optical deposition	1564 nm	6.6 μs	61.0 kHz	3.7 mW	63.9 nJ	[44]
EDFL	Direct optical deposition on tapered fibre	1560 nm	7 μs	37.3 kHz	0.6 mW	-	[45]
EDFL	Composite film	1548 – 1552 nm	2.72 μs	72.25 kHz	16.6 mW	229.74 nJ	[51]
YDFL	Composite film	1094 nm	3.5 μs	-	-	-	[49]
YDFL	Composite film		2.65 μs	58.95 kHz	7.92 mW	2.98 μJ	[47]

References

[1] A. Einstein, "Zur Quantentheorie der Strahlung," *Physikalische Zeitschrift*, vol. 18, pp. 121-128, 1917.

[2] T. H. Maiman, "Stimulated optical radiation in ruby," 1960.

[3] R. N. Hall, G. E. Fenner, J. D. Kingsley, T. J. Soltys, and R. O. Carlson, "Coherent Light Emission From GaAs Junctions," *Physical Review Letters*, vol. 9, pp. 366-368, 1962.

[4] E. Snitzer, "Optical Maser Action of Nd^{3+} in a Barium Crown Glass," *Physical Review Letters*, vol. 7, pp. 444-446, 1961.

[5] J. Stone, C. Burrus, A. Dentai, and B. Miller, "Nd: YAG single-crystal fiber laser: Room-temperature cw operation using a single LED as an end pump," *Applied Physics Letters*, vol. 29, pp. 37-39, 1976.

[6] J. T. Verdeyen, *Laser Electronics*: Prentice Hall, 1995.

[7] J. Wilson and J. F. B. Hawkes, *Lasers, principles and applications*: Prentice Hall, 1987.

[8] A. E. Siegman, *Lasers*: Mill Valley: University Science Books, 1986.

[9] O. Svelto, *Principles of Lasers*, 3rd ed.: New York: Plenum, 1989.

[10] G. Spühler, R. Paschotta, R. Fluck, B. Braun, M. Moser, G. Zhang, *et al.*, "Experimentally confirmed design guidelines for passively Q-switched microchip lasers using semiconductor saturable absorbers," *JOSA B*, vol. 16, pp. 376-388, 1999.

[11] J. Zayhowski and P. Kelley, "Optimization of Q-switched lasers," *Quantum Electronics, IEEE Journal of*, vol. 27, pp. 2220-2225, 1991.

[12] R. Paschotta and U. Keller, "Passive mode locking with slow saturable absorbers," *Applied Physics B*, vol. 73, pp. 653-662, 2001/11/01 2001.

[13] U. Hofmann, "Graphit und Graphitverbindungen," in *Ergebnisse der Exakten Naturwissenschaften*, F. Hund and F. Trendelenburg, Eds., ed: Springer Berlin Heidelberg, 1939, pp. 229-256.

[14] D. R. Dreyer, S. Park, C. W. Bielawski, and R. S. Ruoff, "The chemistry of graphene oxide," *Chemical Society Reviews*, vol. 39, pp. 228-240, 2010.

[15] G. Ruess, *Monatsh. Chem.* , vol. 76, pp. 381-417, 1946.

[16] W. Scholz and H. P. Boehm, "Untersuchungen am Graphitoxid. VI. Betrachtungen zur Struktur des Graphitoxids," *Zeitschrift für anorganische und allgemeine Chemie*, vol. 369, pp. 327-340, 1969.

[17] T. Nakajima, A. Mabuchi, and R. Hagiwara, "A new structure model of graphite oxide," *Carbon*, vol. 26, pp. 357-361, 1988.

[18] T. Nakajima and Y. Matsuo, "Formation process and structure of graphite oxide," *Carbon*, vol. 32, pp. 469-475, 1994.

[19] H. He, J. Klinowski, M. Forster, and A. Lerf, "A new structural model for graphite oxide," *Chemical Physics Letters*, vol. 287, pp. 53-56, 1998.

[20] H. He, T. Riedl, A. Lerf, and J. Klinowski, "Solid-State NMR Studies of the Structure of Graphite Oxide," *The Journal of Physical Chemistry*, vol. 100, pp. 19954-19958, 1996/01/01 1996.

[21] A. Lerf, H. He, M. Forster, and J. Klinowski, "Structure of Graphite Oxide Revisited‖," *The Journal of Physical Chemistry B*, vol. 102, pp. 4477-4482, 1998/06/01 1998.

[22] M. Mermoux, Y. Chabre, and A. Rousseau, "FTIR and 13C NMR study of graphite oxide," *Carbon*, vol. 29, pp. 469-474, 1991.

[23] A. Lerf, H. He, T. Riedl, M. Forster, and J. Klinowski, "13C and 1H MAS NMR studies of graphite oxide and its chemically modified derivatives," *Solid State Ionics*, vol. 101–103, Part 2, pp. 857-862, 1997.

[24] A. Buchsteiner, A. Lerf, and J. Pieper, "Water Dynamics in Graphite Oxide Investigated with Neutron Scattering," *The Journal of Physical Chemistry B,* vol. 110, pp. 22328-22338, 2006/11/01 2006.

[25] A. Lerf, A. Buchsteiner, J. Pieper, S. Schöttl, I. Dekany, T. Szabo, *et al.*, "Hydration behavior and dynamics of water molecules in graphite oxide," *Journal of Physics and Chemistry of Solids,* vol. 67, pp. 1106-1110, 5// 2006.

[26] H. P. Boehm and W. Scholz, "Der „Verpuffungspunkt" des Graphitoxids," *Zeitschrift für anorganische und allgemeine Chemie,* vol. 335, pp. 74-79, 1965.

[27] W. Cai, R. D. Piner, F. J. Stadermann, S. Park, M. A. Shaibat, Y. Ishii, *et al.*, "Synthesis and solid-state NMR structural characterization of 13C-labeled graphite oxide," *Science,* vol. 321, pp. 1815-1817, 2008.

[28] W. Gao, L. B. Alemany, L. Ci, and P. M. Ajayan, "New insights into the structure and reduction of graphite oxide," *Nature chemistry,* vol. 1, pp. 403-408, 2009.

[29] T. Szabó, O. Berkesi, P. Forgó, K. Josepovits, Y. Sanakis, D. Petridis, *et al.*, "Evolution of surface functional groups in a series of progressively oxidized graphite oxides," *Chemistry of Materials,* vol. 18, pp. 2740-2749, 2006.

[30] D. W. Boukhvalov and M. I. Katsnelson, "Modeling of graphite oxide," *Journal of the American Chemical Society,* vol. 130, pp. 10697-10701, 2008.

[31] T. Ando, Y. Zheng, and H. Suzuura, "Dynamical conductivity and zero-mode anomaly in honeycomb lattices," *Journal of the Physical Society of Japan,* vol. 71, pp. 1318-1324, 2002.

[32] A. Kuzmenko, E. Van Heumen, F. Carbone, and D. Van Der Marel, "Universal optical conductance of graphite," *Physical Review Letters,* vol. 100, p. 117401, 2008.

[33] Z. Li, E. A. Henriksen, Z. Jiang, Z. Hao, M. C. Martin, P. Kim, *et al.*, "Dirac charge dynamics in graphene by infrared spectroscopy," *Nature Physics,* vol. 4, pp. 532-535, 2008.

[34] K. F. Mak, M. Y. Sfeir, Y. Wu, C. H. Lui, J. A. Misewich, and T. F. Heinz, "Measurement of the optical conductivity of graphene," *Physical Review Letters,* vol. 101, p. 196405, 2008.

[35] R. Nair, P. Blake, A. Grigorenko, K. Novoselov, T. Booth, T. Stauber, *et al.*, "Fine structure constant defines visual transparency of graphene," *Science,* vol. 320, pp. 1308-1308, 2008.

[36] P. A. George, J. Strait, J. Dawlaty, S. Shivaraman, M. Chandrashekhar, F. Rana, *et al.*, "Ultrafast Optical-Pump Terahertz-Probe Spectroscopy of the Carrier Relaxation and Recombination Dynamics in Epitaxial Graphene," *Nano Letters,* vol. 8, pp. 4248-4251, 2008/12/10 2008.

[37] J. M. Dawlaty, S. Shivaraman, M. Chandrashekhar, F. Rana, and M. G. Spencer, "Measurement of ultrafast carrier dynamics in epitaxial graphene," *Applied Physics Letters,* vol. 92, p. 042116, 2008.

[38] R. N. Zitter, "Saturated Optical Absorption Through Band Filling In Semiconductors," *Applied Physics Letters,* vol. 14, pp. 73-74, 1969.

[39] Q. Bao, H. Zhang, Y. Wang, Z. Ni, Y. Yan, Z. X. Shen, *et al.*, "Atomic-Layer Graphene as a Saturable Absorber for Ultrafast Pulsed Lasers," *Advanced Functional Materials,* vol. 19, pp. 3077-3083, 2009.

[40] Z. Luo, P. M. Vora, E. J. Mele, A. T. C. Johnson, and J. M. Kikkawa, "Photoluminescence and band gap modulation in graphene oxide," *Applied Physics Letters,* vol. 94, pp. -, 2009.

[41] X. Zhao, Z.-B. Liu, W.-B. Yan, Y. Wu, X.-L. Zhang, Y. Chen, *et al.*, "Ultrafast carrier dynamics and saturable absorption of solution-processable few-layered graphene oxide," *Applied Physics Letters,* vol. 98, pp. -, 2011.

[42] Z. Luo, M. Zhou, J. Weng, G. Huang, H. Xu, C. Ye, *et al.*, "Graphene-based passively Q-switched dual-wavelength erbium-doped fiber laser," *Optics Letters,* vol. 35, pp. 3709-3711, 2010/11/01 2010.

[43] H. Ahmad, A. Z. Zulkifli, K. Thambiratnam, and S. W. Harun, "2.0-μm Q-Switched Thulium-Doped Fiber Laser With Graphene Oxide Saturable Absorber," *Photonics Journal, IEEE,* vol. 5, pp. 1501108-1501108, 2013.

[44] H. Ahmad, F. D. Muhammad, M. Z. Zulkifli, and S. W. Harun, "Graphene-Oxide-Based Saturable Absorber for All-Fiber Q-Switching With a Simple Optical Deposition Technique," *Photonics Journal, IEEE,* vol. 4, pp. 2205-2213, 2012.

[45] L. Gao, T. Zhu, and J. Zeng, "Wavelength Spacing Tunable, Multiwavelength Q-Switched Mode-Locked Laser Based on Graphene-Oxide-Deposited Tapered Fiber," *arXiv preprint arXiv:1401.1299,* 2014.

[46] J. Lee, J. Koo, P. Debnath, Y. Song, and J. Lee, "A Q-switched, mode-locked fiber laser using a graphene oxide-based polarization sensitive saturable absorber," *Laser Physics Letters,* vol. 10, p. 035103, 2013.

[47] J. Zhao, Y. Wang, P. Yan, S. Ruan, Y. Tsang, G. Zhang, *et al.*, "An Ytterbium-doped fiber laser with dark and Q-switched pulse generation using graphene-oxide as saturable absorber," *Optics Communications,* vol. 312, pp. 227-232, 2014.

[48] X. Li, Q. Wang, Y. Tang, Z. Yan, Y. Wang, B. Meng, *et al.*, "Broadband saturable absorption of graphene oxide thin film and its application in pulsed fiber lasers," 2014.

[49] L. Liu, H. T. Hattori, E. G. Mironov, and A. Khaleque, "Composite chromium and graphene oxide as saturable absorber in ytterbium-doped Q-switched fiber lasers," *Applied Optics,* vol. 53, pp. 1173-1180, 2014.

[50] C. Feng, D. Liu, and J. Liu, "Graphene oxide saturable absorber on golden reflective film for Tm: YAP Q-switched mode-locking laser at 2 μm," *Journal of Modern Optics,* vol. 59, pp. 1825-1828, 2012.

[51] Z. Jun-Qing, W. Yong-Gang, Y. Pei-Guang, R. Shuang-Chen, C. Jian-Qun, D. Ge-Guo, *et al.*, "Graphene-oxide-based Q-switched fiber laser with stable five-wavelength operation," *Chinese Physics Letters,* vol. 29, p. 114206, 2012.

[52] C. Liu, C. Ye, Z. Luo, H. Cheng, D. Wu, Y. Zheng, *et al.*, "High-energy passively Q-switched 2 μm Tm 3+-doped double-clad fiber laser using graphene-oxide-deposited fiber taper," *Optics express,* vol. 21, pp. 204-209, 2013.

[53] H. Ahmad, M. R. K. Soltanian, C. H. Pua, M. Alimadad, and S. W. Harun, "Photonic crystal fiber based dual-wavelength Q-switched fiber laser using graphene oxide as a saturable absorber," *Applied Optics,* vol. 53, pp. 3581-3586, 2014/06/01 2014.